Available online at www.sciencedirect.com
ScienceDirect
Trans. Nonferrous Met. Soc. China 34(2024) 2972−2986
Transactions of Nonferrous Metals Society of China
www.tnmsc.cn

In-situ building of multiscale porous NiFeZn/NiZn-Ni heterojunction for superior overall water splitting

Ya-xin LI[1], Hong-xiao YANG[1], Qiu-ping ZHANG[1],
Tian-zhen JIAN[1], Wen-qing MA[1], Cai-xia XU[1], Qiu-xia ZHOU[2]

1. Institute for Advanced Interdisciplinary Research (iAIR), University of Jinan, Jinan 250022, China;
2. School of Medical Information and Engineering, Southwest Medical University, Luzhou 646000, China

Received 22 February 2023; accepted 12 October 2023

Abstract: The development of efficient nonprecious bifunctional electrocatalysts for water electrolysis is crucial to enhance the sluggish kinetics of the oxygen evolution reaction (OER) and hydrogen evolution reaction (HER). A self-supporting, multiscale porous NiFeZn/NiZn-Ni catalyst with a triple interface heterojunction on nickel foam (NF) (NiFeZn/NiZn-Ni/NF) was in-situ fabricated using an electroplating−annealing−etching strategy. The unique multi-interface engineering and three-dimensional porous scaffold significantly modify the mass transport and electron interaction, resulting in superior bifunctional electrocatalytic performance for water splitting. The NiFeZn/NiZn-Ni/NF catalyst demonstrates low overpotentials of 187 mV for HER and 320 mV for OER at a current density of 600 mA/cm², along with high durability over 150 h in alkaline solution. Furthermore, an electrolytic cell assembled with NiFeZn/NiZn-Ni/NF as both the cathode and anode achieves the current densities of 600 and 1000 mA/cm^2 at cell voltages of 1.796 and 1.901 V, respectively, maintaining the high stability at 50 mA/cm^2 for over 100 h. These findings highlight the potential of NiFeZn/NiZn-Ni/NF as a cost-effective and highly efficient bifunctional electrocatalyst for overall water splitting.

Key words: NiFeZn alloy; multiple interface; porous structure; dealloying; overall water splitting

1 Introduction

The excessive consumption of fossil fuels and the resulting environmental pollution have become primary global challenges, urging the exploration and development of renewable clean energy sources [1−3]. Hydrogen is a promising alternative to fossil fuels due to its environmental benefits and high energy density [4−6]. Among various hydrogen production techniques, electrocatalytic water splitting stands out as a promising approach because it utilizes recyclable water sources and produces zero carbon emissions. However, slow hydrogen evolution reaction (HER) and oxygen evolution reaction (OER) kinetics impede its commercial application [7−9]. This presents a strategic opportunity to develop efficient and cost-effective electrocatalysts for HER and OER in water splitting. In particular, bifunctional electrocatalysts are preferable as they can reduce the overall cost of the electrolytic system by simplifying the fabrication of electrode materials.

Significant attention has been paid to exploring nonprecious metal-based electrocatalysts for water splitting due to their low cost and respectable activities. Ni-based electrocatalysts have presented excellent OER and HER activities

Corresponding author: Cai-xia XU, Tel/Fax: +86-531-82767033, E-mail: chm_xucx@ujn.edu.cn;
Qiu-xia ZHOU, E-mail : qxzhou2022@swmu.edu.cn
DOI: 10.1016/S1003-6326(24)66589-1

through the component and microstructure engineering [10,11]. Combining Ni with elements like Co, Fe, and Mo to form multinary alloys can optimize electron structure and enhance synergistic effects, thus improving the bifunctional activities. For example, ternary NiCoFe alloy nanosheets displayed exceptional bifunctional activities with low overpotentials of 220 and 239 mV for HER and OER at 10 mA/cm^2 in 1.0 mol/L KOH electrolyte, respectively, indicating high catalytic efficiency [12]. GAO et al [13] found that Ni−Co−Mo-based bifunctional electrocatalysts outperformed Ni, Co, Ni−Mo, and Co−Mo catalysts in alkaline electrolyte. Consequently, tailoring ternary alloy components has been one effective protocol to enhance the HER and OER bifunctional catalytic activities [14].

Microstructure is crucial for promoting the mass transport and active site accessibility [15]. Three-dimensional (3D) porous architecture offers superior electrocatalysis reaction kinetics due to more efficient mass transfer and robust structural stability coming from the interconnected skeleton and the rich hollow pore channels [16]. Creating structural defects like corners, edges, vacancies, and grain boundaries during pore formation can boost the intrinsic catalytic activity of electrocatalysts [17,18]. Moreover, interface coupling has been witnessed to be another widely-adopted strategy to improve the catalytic activity because the multiple interface architecture can help to further regulate the electronic structure, facilitate the mass transfer, and optimize reaction intermediate adsorption and desorption [19,20].

Building on these insights, we deploy a scalable dealloying strategy for in-situ building of the porous NiFeZn/NiZn-Ni with triple interface heterojunction on nickel foam (NF), i.e. NiFeZn/NiZn-Ni/NF, as the bifunctional electrocatalyst in water splitting. The proposed dealloying protocol involves electrodeposition of NiFeZn coating on NF, followed by annealing and selective Zn corrosion, without complex or hazardous operations [21−23]. The NiFeZn/NiZn-Ni/NF features efficient mass transport, abundant catalytic sites, and robust structural stability due to its multilevel porous structure and multiple interface coupling. The NiFeZn/NiZn-Ni/NF shows outstanding electrocatalytic performance, rapid reaction kinetics, and long-term durability for both HER and OER in alkaline electrolyte. It achieves significantly lower cell potential in electrochemical water splitting compared to similar electrocatalysts. Our work presents a promising method for constructing low-cost, free-standing, multiscale porous alloy heterostructures with outstanding bifunctional performances for water splitting.

2 Experimental

2.1 Chemicals

Pt/C (20 wt.%) and RuO_2 (99.9%) catalysts were obtained from Sigma Aldrich Chemical Reagent Co., Ltd. Other reagents, including KOH, HCl, NaOH, $NiSO_4·6H_2O$, $FeSO_4·7H_2O$, $ZnSO_4·6H_2O$, and $C_6H_5Na_3O_7·2H_2O$, were purchased from Shanghai Sinopharm Chemical Reagent Ltd., Co., China. All chemicals were used as-received without further purification and were intended for analytical purposes. The purity of these chemicals is crucial for reproducibility and has been maintained as per the supplier's specifications.

2.2 Preparation of NiFeZn/NiZn-Ni/NF

NF was pretreated by sonicating in 3 mol/L HCl solution for 30 min, followed by cleaning with anhydrous ethanol and deionized water. The electrodeposition of NiFeZn was performed in a three-electrode cell for 1 h at −1.7 V (vs saturated calomel electrode (SCE)) in a mixed solution of 0.2 mol/L $ZnSO_4$, 0.005 mol/L $NiSO_4$, 0.06 mol/L $FeSO_4$, and 0.4 mol/L $C_6H_5Na_3O_7$. The cleaned NF (1 cm × 2 cm × 1 mm) served as the working electrode, with a Pt plate as the counter electrode and SCE as the reference electrode. The resultant NiFeZn/NF sample was then annealed in a tube furnace under flowing Ar atmosphere at 450 °C for 10 h with a heating rate of 5 °C/min. Subsequently, the NiFeZn/NiZn/NF sample was etched in the 1.0 mol/L NaOH solution at room temperature for 12, 24, and 48 h to obtain NiFeZn/NiZn-Ni/NF-12h, NiFeZn/NiZn-Ni/NF-24h, and NiFeZn/NiZn-Ni/NF-48h samples, respectively. For comparison, the NiZn-Ni/NF sample was also prepared under the same conditions in a mixed solution of 0.2 mol/L $ZnSO_4$ and 0.4 mol/L $C_6H_5Na_3O_7$.

2.3 Characterization

X-ray diffraction (XRD) using a Bruker D8 advanced with Cu K_α radiation (step rate: 0.02 (°)/s)

was utilized to analyze the crystal structure. Transmission electron microscope (TEM; JEOL JEM-ARF200F) and scanning electron microscope (SEM; Hitachi Regulus 8100) with an X-sight energy dispersive X-ray spectrometer (EDS; Oxford INCA) were used to examine the microstructures and compositions. X-ray photoelectron spectroscope (XPS; ESCALAB 250) was adopted to analyze the chemical states. The Brunauer−Emmett−Teller (BET) method (Quadrasorb SI-MP) was used to measure the pore size distribution of samples.

2.4 Electrochemical tests

All electrocatalytic tests were carried out in a three-electrode system in 1.0 mol/L KOH solution. NiFeZn/NiZn-Ni/NF samples with a geometric area of 0.2 cm^2 (1 cm × 0.2 cm) were directly used as the working electrode. A graphite rod was utilized as the counter electrode, with a mercuric oxide electrode (MOE) as the reference electrode for all tests. Before measurements, the electrolyte was purged with pure N_2 for 30 min to eliminate dissolved oxygen. All potentials were given according to a reversible hydrogen electrode (RHE) using the equation: $\varphi_{RHE}=\varphi_{MOE}+0.924$. Linear sweep voltammetry (LSV) tests with 90% *iR* compensation were conducted at a scan rate of 5 mV/s. Cyclic voltammetry (CV) was used to determine the double-layer capacitance (C_{dl}) in the potential range of 1.124−1.224 V (vs RHE) at different scan rates. Electrochemical impedance spectroscopy (EIS) test was implemented at a fixed overpotential from 0.01 to 100 kHz with an amplitude of 10 mV. Commercial Pt/C and RuO_2 were dropped onto NF (1 cm × 0.2 cm) with a loading mass of ~4.0 mg/cm^2 for HER and OER tests, respectively. Durability tests were conducted via chronoamperometry at a fixed potential. Overall water splitting tests were operated in 1.0 mol/L KOH solution using a two-electrode system. The commercial Pt/C and RuO_2 as benchmarks for HER and OER tests serve as control experiments.

3 Results and discussion

3.1 Morphology and structure of NiFeZn/NiZn-Ni/NF sample

Figure 1 illustrated the preparation procedure of NiFeZn/NiZn-Ni/NF sample. The NF was selected as the substrate due to its interconnected hollow channels and 3D skeleton, which represents one type of robust and high surface area supports. A layer of NiFeZn alloy was electroplated on NF followed by annealing in Ar atmosphere at 450 °C for 10 h. Due to the low melting point of Zn, a part of Zn atoms in NiFeZn alloy rapidly diffused into the surface layer of NF. After selectively dissolving partial Zn atoms from the annealed sample, the upper electroplated coating evolved into bimodal porous NiFeZn alloy, while the bottom layer within NF permeated by Zn atoms assembled into bimodal porous NiZn-Ni heterostructure. The bimodal porous double-layered heterojunction structure not only further enlarged the surface area by the construction of mesopores but also generated rich interface coupling.

Figure S1 in Supporting Information (SI) showed the SEM images, which were utilized to demonstrate the structural evolution from NF to the final product. Compared with the smooth surface of the 3D skeleton for the NF (Fig. S1(a) in SI), the irregularly granular layer formed after electroplating (Fig. S1(b) in SI), in which the Ni/Fe/Zn molar ratio in NiFeZn was 2.90:2.87:94.23 as confirmed by EDS data (Fig. S1(c) in SI). After the annealing process, the surface of the skeleton became much rougher (Fig. S1(d) in SI). By selectively etching Zn atoms in 1.0 mol/L NaOH solution for 24 h,

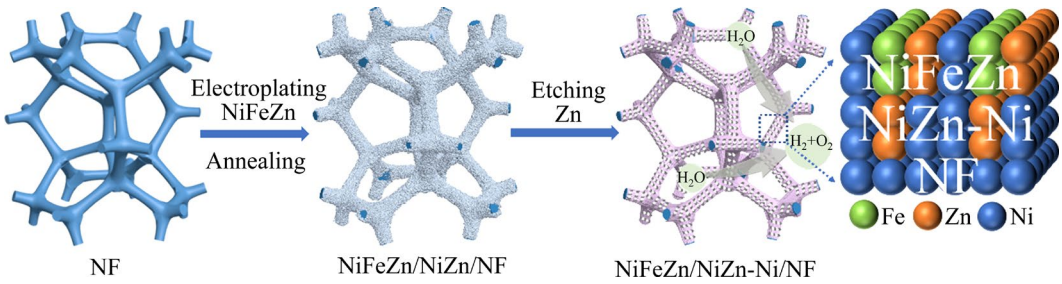

Fig. 1 Schematic diagram showing fabrication of double-layered multiscale porous NiFeZn/NiZn-Ni heterojunction with triple interface grown on NF

numerous open pores were produced with the ligament diameter about 200 nm (Figs. 2(a, b)). Moreover, by peeling off the surface layer through ultrasonic treatment, the double-layered porous structure can be clearly observed [23]. The cross-sectional SEM image shows that the upper NiFeZn alloy layer has a thickness of ~3 μm (Fig. 2(c)). According to the element mappings in the SEM image (Figs. 2(c_1−c_3)), it can be observed that Fe atoms are distributed merely in the upper porous layer, while Ni and Zn atoms are uniformly dispersed throughout the two porous layers. The above results substantially indicate that the nanoporous structure of the upper layer is composed of NiFeZn alloy, and the bottom layer is made up of NiZn intermetallic and Ni heterojunction. The phase constituent was further confirmed by XRD. Besides, the corresponding EDS data of different regions in Fig. 2(c) also further confirm the above results (Fig. S2 in SI).

Figure 2(d) presents the TEM image of the slices peeled off from the NiFeZn/NiZn-Ni/NF-24h sample. The peeled slices came from the upper layer of NiFeZn alloy because they were obtained by sonicating the sample for a long time at ice temperature. It can be observed that there are a number of large pores (as denoted by the yellow square), which correspond to the large pores on the surface of the upper NiFeZn alloy. Figure 2(e) shows the enlarged TEM image, in which a large number of bright regions can be distinguished as marked by the green square. From an enlarged TEM image of the marked region in Fig. 2(f), it is evident that there are numerous pores with a typical size of around 6 nm [23]. Additionally, the Barret−Joyner−Halenda (BJH) pore size analysis result for NiFeZn/NiZn-Ni/NF-24h (Fig. S3 in SI) shows that the majority of the pores are approximately 6 nm along with some pores of 100−200 nm, which is well coincident with the electron microscopic observation. In the high-resolution TEM (HRTEM) image in Fig. 2(g), the continuous ordered fringes can be determined to be the (110) plane of NiFeZn alloy. The corresponding selected area electron diffraction (SAED) is shown in Fig. 2(h), in which a sequence of different diffraction rings can be identified to be (222), (110), and (200) planes of NiFeZn alloy, respectively. The above observations indicate that the diffusion of low-melting Zn upon annealing followed by selective dissolution of

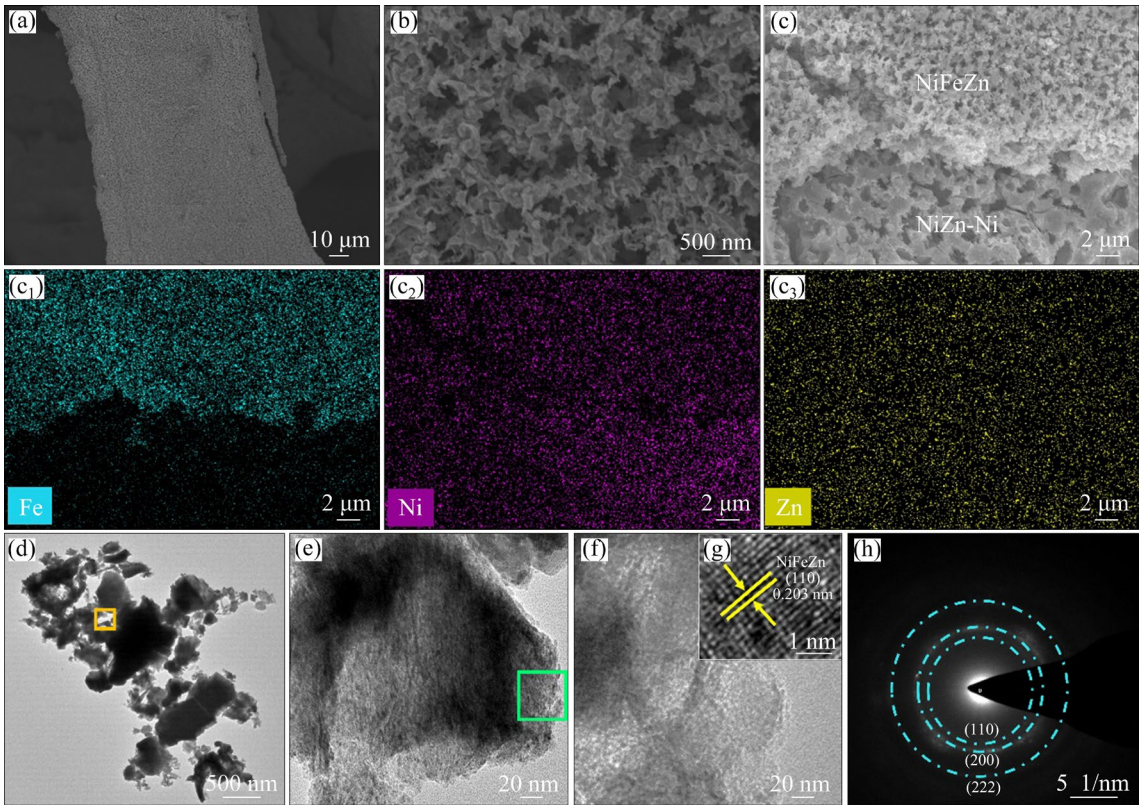

Fig. 2 Sufacial (a, b), cross-sectional (c) SEM images, corresponding element mappings of Fe (c_1), Ni (c_2) and Zn (c_3) elements, TEM (d−f) and HRTEM (g) images, and SAED image (h) of NiFeZn/NiZn-Ni/NF-24h sample

partial Zn atoms can straightforwardly in-situ create the bimodal porous double-layered NiFeZn and NiZn-Ni heterojunction with triple interface.

In addition, the formation and evolution of the NiFeZn/NiZn-Ni/NF were further examined by monitoring the effects of corrosion time on the resultant structure. After etching for only 12 h, numerous uniform holes gradually emerged on the sample surface (Figs. S4(a, d) in SI). When further extending the dealloying time to 48 h, the nanoporous structure underwent accumulation along with ligament coarsening (Figs. S4(b, e) in SI). By comparison, dealloying for 24 h is beneficial for achieving a more uniform porous structure. Besides, the SEM image and the EDS data (Figs. S4(c, f) in SI) show that the NiZn-Ni/NF sample also has the similar porous structure, which provides the material basis for the performance comparison for overall water splitting.

The phase structure and component of the NiFeZn/NiZn-Ni/NF-24h sample were further investigated through XRD. After electroplating NiFeZn on NF, a set of new diffraction peaks appeared compared with those of NF (JCPDS No. 04-0850) in Fig. S5(a) in SI. The diffraction peaks at 2θ values of around 35.0°, 38.9°, 43.2°, 54.3°, and 70.1° could be indexed to metallic Zn (JCPDS No. 65-5973). The characteristic peaks located at 2θ values of 43.3°, 57.2°, 67.9°, 76.4°, and 84.5° should be assigned to NiZn intermetallic (JCPDS No. 06-0672), while the peaks at 2θ values of 44.6°, 65.0°, and 82.3° should be ascribed to the formation of NiFeZn alloy with a similar phase structure to that of (Fe,Ni) alloy (JCPDS No. 37-0474) in view of the high content of Zn. Many remaining diffraction peaks matched well with those of the $NiZn_3$ intermetallic (JCPDS No. 47-1019) [23]. Upon annealing at 450 °C for 10 h, newly emerged diffraction peaks at 2θ values of 43.5°, 63.2°, and 79.8° corresponded to the standard $Fe_{6.8}Zn_{3.2}$ pattern (JCPDS No. 65-4399), while the additional seven diffraction peaks should be attributed to ZnO (JCPDS No. 36-1451) owing to the easy oxidation of surface Zn atoms during the annealing or drying process (Fig. S5(b) in SI). After etching Zn atoms, the resulting sample solely displays the diffraction peaks of Ni, NiZn intermetallic, and NiFeZn alloy as shown in Fig. 3, indicating the in-situ construction of NiFeZn/NiZn-Ni alloy anchored on NF.

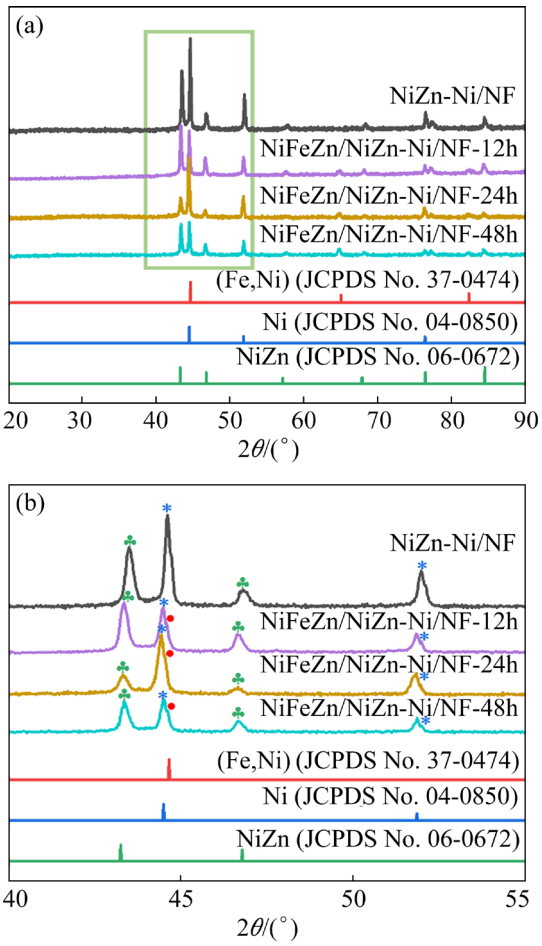

Fig. 3 Full (a) and local magnified (b) XRD patterns of NiZn-Ni/NF and NiFeZn/NiZn-Ni/NF samples with different etching time

XPS was utilized to analyze the chemical states for the NiFeZn/NiZn-Ni/NF-24h sample. As displayed in the Ni 2p spectrum (Fig. 4(a)), the metallic Ni displays the peaks at 852.60 and 869.48 eV accompanied with the evident negative shift of ~0.42 eV in comparison with the standard Ni [23]. Meanwhile, two strong peaks at 855.80 and 873.42 eV with two satellite peaks correspond to the Ni^{2+} species [24], while the peaks at 857.72 and 875.80 eV are indexed to Ni^{3+} species [25], illustrating the existence of nickel oxide and hydroxides on the sample surface. From the Fe 2p spectrum in Fig. 4(b), the peaks at 707.10 and 720.20 eV belong to metallic Fe in the NiFeZn alloy [26], in which the peaks underwent a positive shift by ~0.30 eV in comparison with that of pure Fe. Besides, the peaks at 710.22 and 724.54, 713.17 and 727.35, 716.89 and 733.38 eV can be attributed to Fe^{2+}, Fe^{3+}, and satellite peaks, respectively [27].

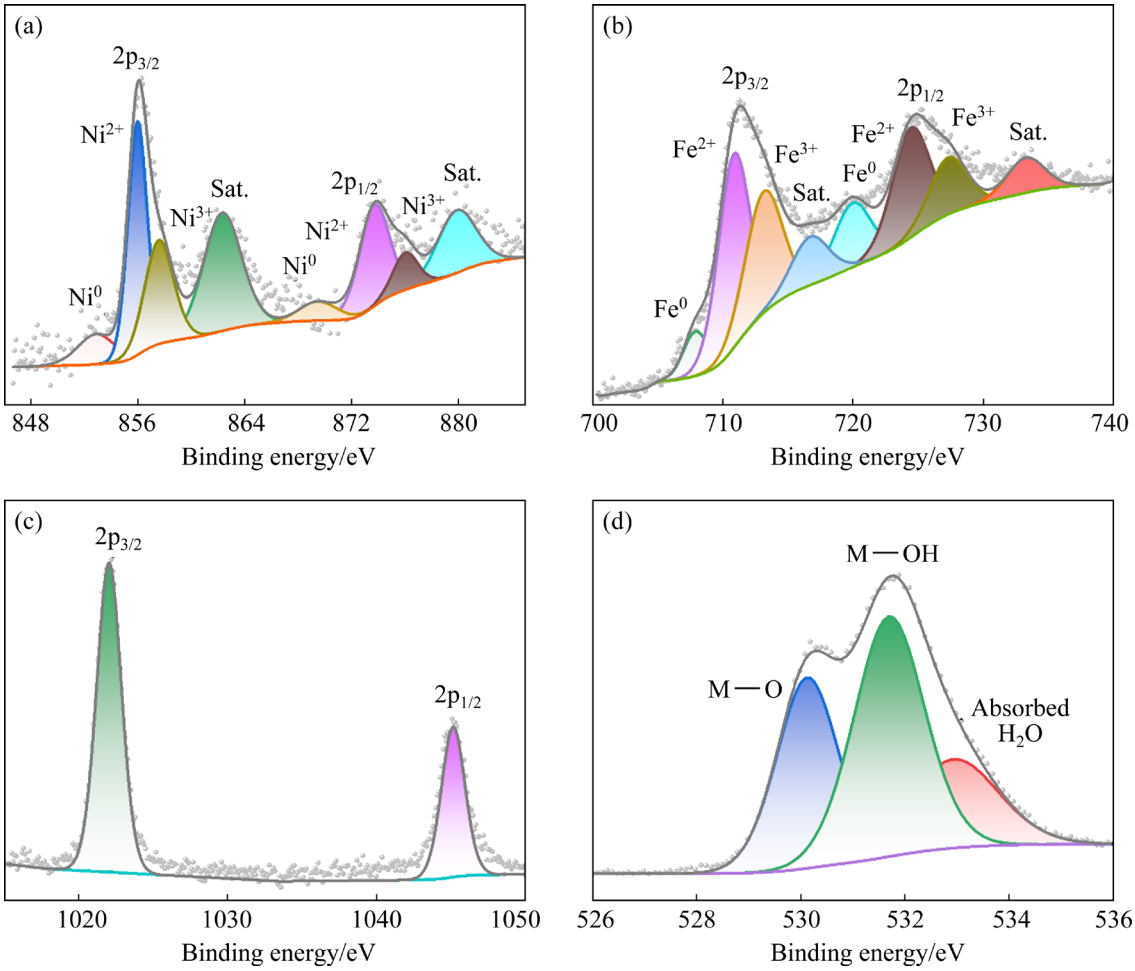

Fig. 4 XPS spectra of NiFeZn/NiZn-Ni/NF-24h sample: (a) Ni 2p; (b) Fe 2p; (c) Zn 2p; (d) O 1s

The presence of Fe^{2+} and Fe^{3+} indicates the existence of iron oxide and/or hydroxides in the sample [28,29]. As for the Zn 2p core level region (Fig. 4(c)), the characteristic peak of Zn $2p_{3/2}$ at 1021.63 eV can be assigned to the metallic Zn along with a positive shift of ~0.46 eV in contrast to that of pure Zn [30]. The obvious core level shifts of Ni, Fe, and Zn in NiFeZn/NiZn-Ni/NF-24h indicate that the multiple interfaces can generate efficient electron modulation, which favors the adsorption/desorption processes of the reaction intermediates during water splitting [31]. In the case of the O 1s spectrum in Fig. 4(d), the peaks located at 529.96, 531.66, and 532.94 eV stem from the metal—oxygen (M—O), metal—hydroxyl (M — OH), and absorbed water on the sample surface, respectively [32,33]. It is obvious that the M—OH groups absorbed on the metal surface are the primary oxygen state [34,35]. All of these observations further confirm the successful fabrication of the NiFeZn/NiZn-Ni/NF sample.

3.2 Catalytic performances of NiFeZn/NiZn-Ni/NF sample for HER

The catalytic performances of the NiFeZn/NiZn-Ni/NF-24h sample for HER were investigated with those of Pt/C/NF, NiZn-Ni/NF, and samples dealloyed for 12 and 48 h for comparison. As shown in Fig. 5(a), Pt/C/NF exhibits the best HER activity at current densities lower than 320 mA/cm² among all catalysts. However, the HER activity of NiFeZn/NiZn-Ni/NF-24h surpasses that of Pt/C/NF at higher current densities. This is because the non-self-supported Pt/C/NF catalyst tends to exfoliate at high current densities, leading to a decay in its HER performance [22]. As presented in Fig. 5(b), NF exhibits the overpotentials of 385 and 422 mV to achieve 600 and 1000 mA/cm² for hydrogen evolution, and the NiZn-Ni/NF displays the corresponding 229 and 276 mV, indicating the construction of NiZn-Ni on the NF surface dramatically enhances the HER activity along with decreased overpotentials. In comparison, the

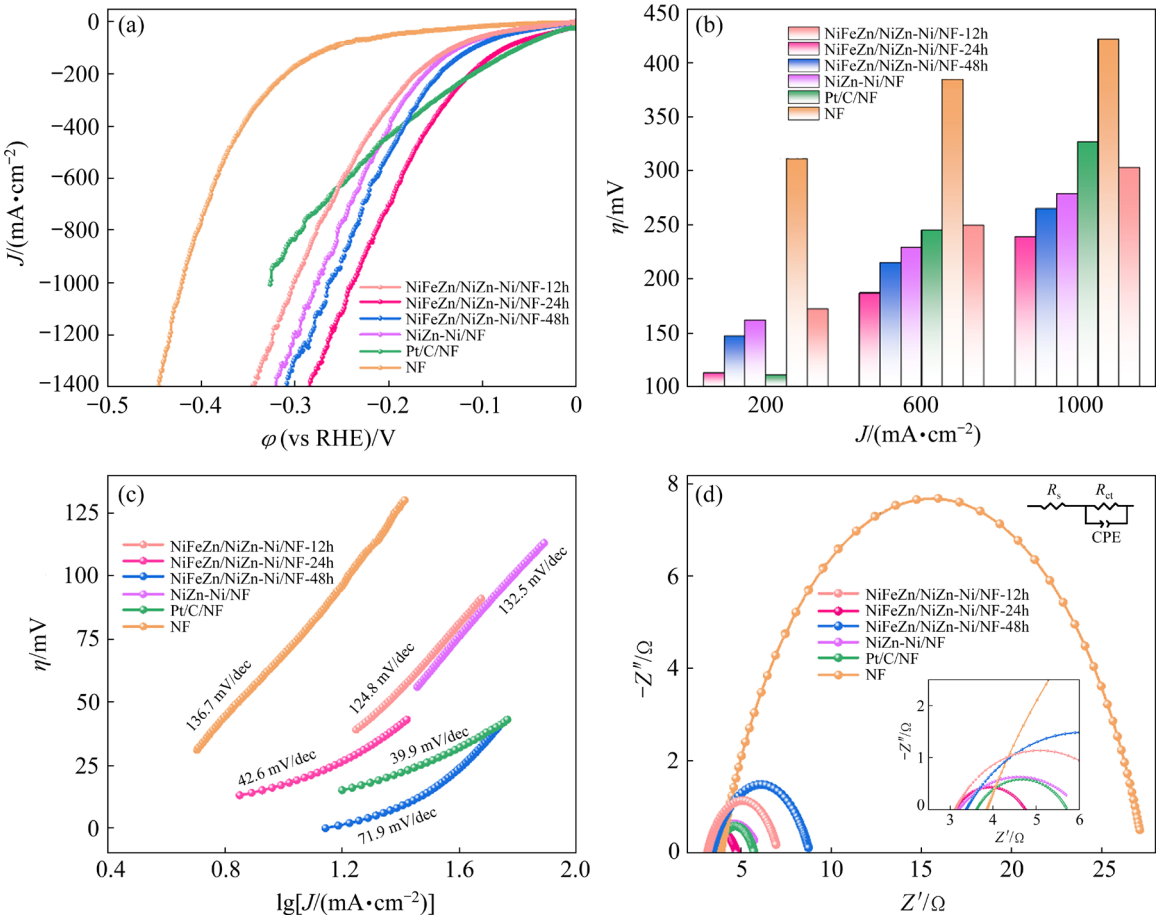

Fig. 5 LSV curves (a), histogram of overpotentials (η) at 200, 600, and 1000 mA/cm^2 (b), Tafel plots (c), and Nyquist plots at overpotential of 200 mV (d) of as-prepared samples for HER

NiFeZn/NiZn-Ni/NF-24h sample displays the overpotentials as low as 187 and 239 mV, respectively, which are much lower than those of NiFeZn/NiZn-Ni/NF-12h sample (250 and 303 mV) and NiFeZn/NiZn-Ni/NF-48h sample (215 and 266 mV). It should be mentioned that they are all much lower than those of NF and NiZn-Ni/NF. On the one hand, the observation above indicates that the construction of NiFeZn alloy layer further boosted the HER activity with the decrease of overpotentials. On the other hand, the double porous NiFeZn and NiZn-Ni layers act as the active sites to generate high HER activity. The Pt/C/NF catalyst demonstrates excellent activities with the lowest overpotentials of 31 and 61 mV at 50 and 100 mA/cm², respectively, but requires a large overpotential of 244 mV to achieve a current density of 600 mA/cm². The NiFeZn/NiZn-Ni/NF-24h sample with the much lower overpotentials for HER is competitive with or even outperforms many other reported nonprecious metal electrocatalysts (Table S1 in SI [36−40]).

To gain more insights into the HER kinetics, the Tafel curves of different catalysts in Fig. 5(c) were derived from their corresponding polarization curves in Fig. 5(a). The reaction mechanism for the HER process in an alkaline solution can be represented by the following steps [36]:

$$H_2O+e+M=H-M+OH^- \quad \text{(Volmer step, 120 mV/dec)} \tag{1}$$

$$H-M+H_2O+e=H_2+OH^-+M \quad \text{(Heyrovsky step, 40 mV/dec)} \tag{2}$$

$$H-M+H-M=H_2+2M \quad \text{(Tafel step, 30 mV/dec)} \tag{3}$$

As seen in Fig. 5(c), the Tafel slope of the as-prepared NiFeZn/NiZn-Ni/NF-24h is as small as 42.6 mV/dec, which is close to that of Pt/C/NF (39.9 mV/dec) and significantly lower than that of NF (136.7 mV/dec) and NiZn-Ni/NF (132.5 mV/dec). This result indicates that the NiFeZn/NiZn-Ni/NF-24h electrode has favorable HER kinetics via a Volmer–Tafel mechanism, where the electrochemical desorption of adsorbed hydrogen is the rate-limiting step [41]. Additionally, EIS test was

performed to further investigate the mass transport efficiency of the NiFeZn/NiZn-Ni/NF samples. As shown in Fig. 5(d), the NiFeZn/NiZn-Ni/NF-24h electrode shows a much smaller charge transfer resistance (R_{ct}) value of 1.4 Ω as compared to 1.9 Ω for NiFeZn/NiZn-Ni/NF-12h, 1.6 Ω for NiFeZn/NiZn-Ni/NF-48h, 2.8 Ω for NiZn-Ni/NF, and 26.4 Ω for NF. This indicates faster mass transfer and much higher electron conductivity upon the construction of NiFeZn and NiZn-Ni double-layer heterojunction during the HER process [27].

Catalytic stability is also a crucial factor for the practical application of HER electrocatalysts. As presented in Fig. 6(a), the durability of NiFeZn/NiZn-Ni/NF-24h and Pt/C/NF was evaluated at an overpotential of 105 mV using chronoamperometric testing. The NiFeZn/NiZn-Ni/NF-24h sample shows only a slight decay over a continuous 150 h test, maintaining a current density around 50 mA/cm². In contrast, Pt/C/NF exhibits severe activity fluctuation,

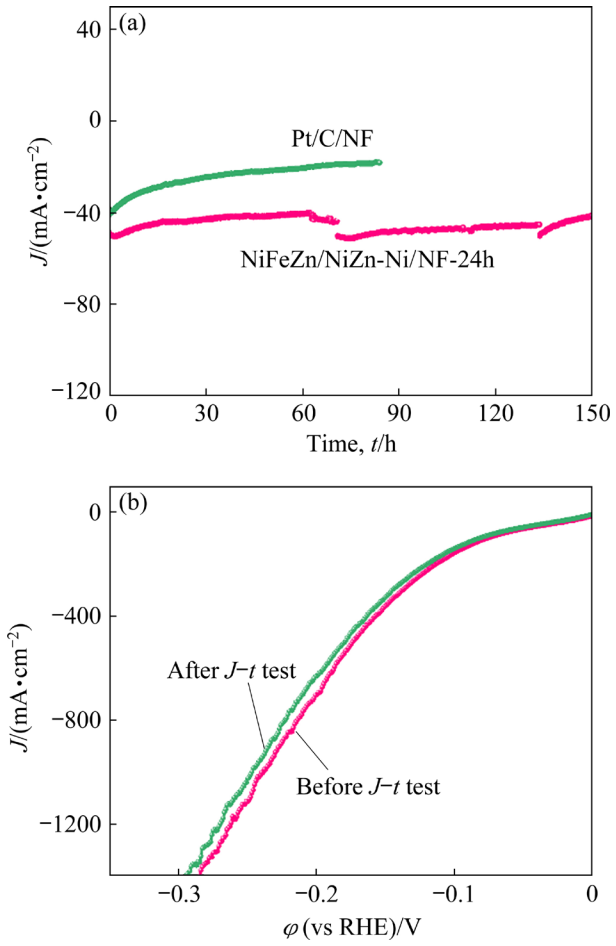

Fig. 6 Chronoamperometric test results of NiFeZn/NiZn-Ni/NF-24h and Pt/C/NF at overpotential of 105 mV for 150 h (a), and LSV curves of NiFeZn/NiZn-Ni/NF-24h before and after *J*–*t* test for HER (b)

retaining only 53.2% of the initial current density. The activity degradation of Pt/C/NF is attributed to the peeling of particle-type catalysts during long-term testing, unlike the seamless integrated electrocatalysts [22]. Furthermore, as shown in Fig. 6(b), the slight deviation of the LSV curves before and after the *J*–*t* test further confirms the outstanding catalytic stability of NiFeZn/NiZn-Ni/NF-24h during HER in alkaline media. Based on the above observations, the NiFeZn/NiZn-Ni/NF-24h sample demonstrates excellent electrocatalytic performance and stability for HER, with low overpotentials, favorable kinetics, and high durability, making it a promising candidate for practical applications in hydrogen production.

3.3 Catalytic performances of NiFeZn/NiZn-Ni/NF sample for OER

The electrocatalytic performances of all catalysts toward OER were further assessed in 1.0 mol/L KOH solution. As shown in Figs. 7(a, b), NiFeZn/NiZn-Ni/NF-24h exhibits the best OER activity with low overpotentials of 320 and 361 mV to afford the large current density of 600 and 1000 mA/cm², which are much lower than those of the other five electrocatalysts. Overpotential is a critical metric as it indicates the efficiency of the catalyst in driving the OER at a given current density. A lower overpotential signifies the more effective catalytic efficiency for NiFeZn/NiZn-Ni/NF-24h catalyst. In particular, the overpotential of NiFeZn/NiZn-Ni/NF-24h for OER in alkaline electrolyte is lower than that of most non-noble metal electrocatalysts reported in recent literatures (Table S2 [36,42−45] in SI). The superior OER activity of NiFeZn/NiZn-Ni/NF-24h compared with that of NiZn-Ni/NF reveals that the in-situ construction of the NiFeZn alloy creates rich highly active sites for OER. Moreover, the triple interface heterostructure can also generate a strong synergistic effect toward electron structure optimization and mass transport [15,20]. Figure 7(c) shows the Tafel plots of the polarization curves from Fig. 7(a) to further clarify the reaction mechanism. The reaction mechanism for the OER process contains four one-electron transfer steps in alkaline media [46]:

$$M+OH^-=MOH+e \quad (4)$$

$$MOH+OH^-=MO+H_2O+e \quad (5)$$

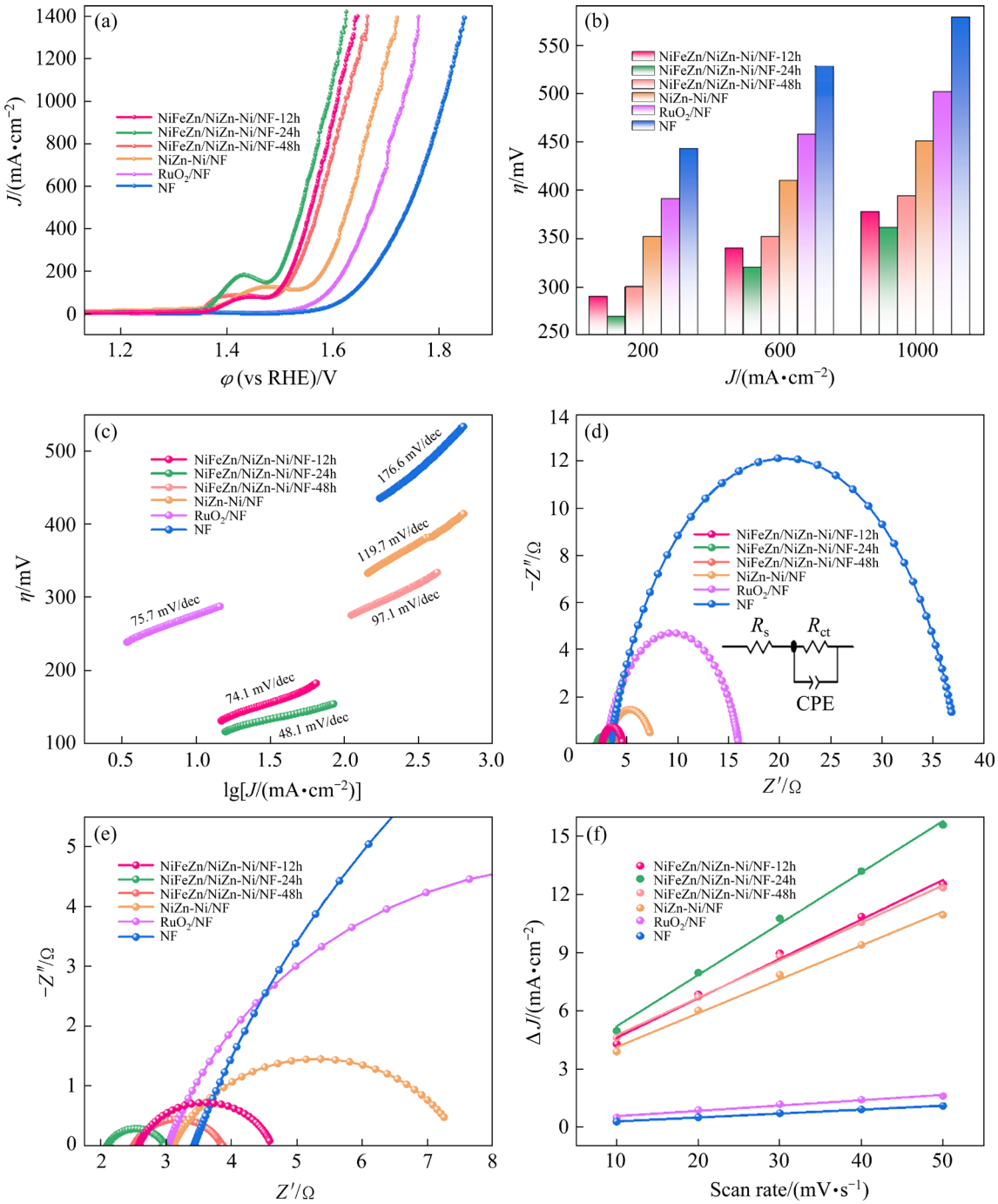

Fig. 7 LSV curves (a), histogram of overpotentials at 200, 600 and 1000 mA/cm^2 (b), Tafel plots (c), Nyquist plots at overpotential of 250 mV (d), enlarged section of Nyquist plots (e), and capacitive current density (ΔJ) at overpotential of 1180 mV and different scan rates (f) of as-prepared samples for OER

$$MO+OH^-=MOOH+e \quad (6)$$

$$MOOH+OH^-=M+O_2+H_2O+e \quad (7)$$

Among all the samples, NiFeZn/NiZn-Ni/NF-24h displays the smallest Tafel slope of 48.1 mV/dec in comparison to NiFeZn/NiZn-Ni/NF-12h (74.1 mV/dec), NiFeZn/NiZn-Ni/NF-48h (97.1 mV/dec), NiZn-Ni/NF (119.7 mV/dec), and NF (176.6 mV/dec) (Fig. 7(c)). According to the commonly accepted oxygen evolution mechanism [46], when the Tafel slope is around 40 mV/dec, the OER kinetics will be significantly impacted by the production of MOOH on the electrode as a result of the reaction between MO and hydroxide. Therefore, the small Tafel slope of NiFeZn/NiZn-Ni/NF-24h means that the creation of

MOOH and its conversion to oxygen are the key rate-determining steps [46].

The mass transfer efficiency of all electrodes for OER was further examined using EIS measurements. According to Figs. 7(d, e), the R_{ct} value of NiFeZn/NiZn-Ni/NF-24h is as low as 0.9 Ω, which is much lower than that of the NiFeZn/NiZn-Ni/NF-12h (1.1 Ω), NiFeZn/NiZn-Ni/NF-48h (1.4 Ω), NiZn-Ni/NF (4.4 Ω), and NF (33.9 Ω), indicating its faster electron transfer kinetics during OER [43]. To further illustrate the activity differences between among electrodes, the C_{dl} values were calculated through the CV measurement to obtain their electrochemical surface area (Figs. 7(f) and S6 in SI) [42]. From Fig. 7(f), the NiFeZn/NiZn-Ni/NF-24h electrode holds the maximum C_{dl} value of 265.7 mF/cm^2 among all samples, which is approximately 1.3, 1.4, 1.5, 9.7, and 13.1 times those of NiFeZn/NiZn-Ni/NF-12h (203.2 mF/cm^2), NiFeZn/NiZn-Ni/NF-48h (192.9 mF/cm^2), NiZn-Ni/NF (174.5 mF/cm^2), RuO_2/NF (27.3 mF/cm^2), and NF (20.3 mF/cm^2), respectively. It is clear that in-situ building of double-layered multiscale porous NiFeZn/NiZn-Ni heterojunction with a triple interface can generate a high density of active sites and significantly improve the OER performances [19,22].

Chronoamperometry measurement was adopted to further assess the long-term stability of the NiFeZn/NiZn-Ni/NF-24h for OER. As displayed in Fig. 8(a), the NiFeZn/NiZn-Ni/NF-24h sample can achieve stable and long-term oxygen evolution with 90.7% activity retention at the overpotential of 220 mV for 150 h. In contrast, RuO_2/NF presents obvious activity degradation with 61.2% of the original current density remaining upon testing for 80 h. According to Fig. S7 in SI, the C_{dl} of the NiFeZn/NiZn-Ni/NF-24h sample still maintained a high value of about 253.3 mF/cm^2 after 150 h OER test, which indicates excellent catalytic durability with nearly no reduction of active sites [22]. The nearly overlapped LSV curves before and after the J–t test in Fig. 8(b) also confirm the superior catalytic durability of NiFeZn/NiZn-Ni/NF-24h for OER.

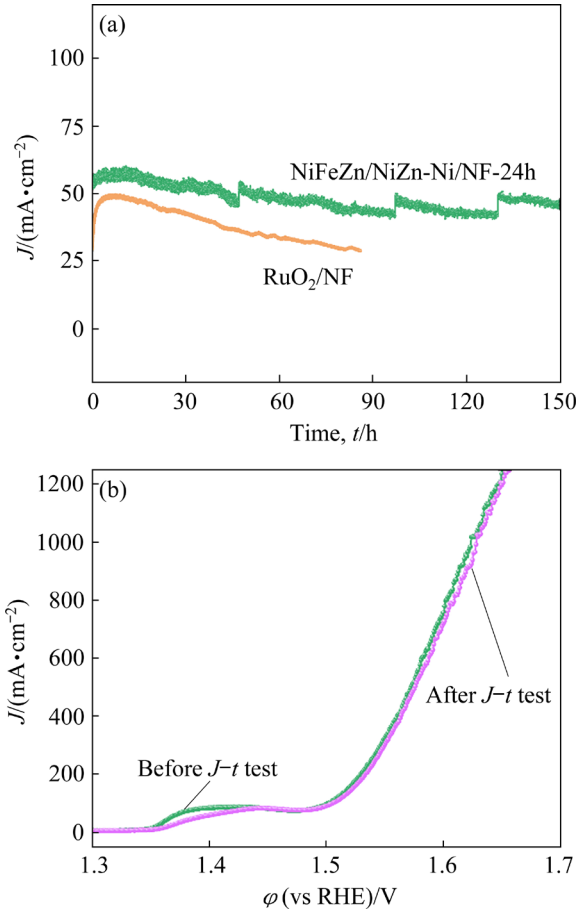

Fig. 8 Chronoamperometric test results of NiFeZn/NiZn-Ni/NF-24h and RuO_2/NF at overpotential of 220 mV for 150 h (a), and LSV curves of NiFeZn/NiZn-Ni/NF-24h before and after J–t test for OER (b)

3.4 Overall water splitting performances of NiFeZn/NiZn-Ni/NF sample

The NiFeZn/NiZn-Ni/NF-24h sample has demonstrated excellent catalytic activities for both the HER and OER. Its performance as a bifunctional electrocatalyst for overall water splitting was further assessed including its cell voltage at a current density of 100 mA/cm^2 and the duration of continuous water electrolysis. As shown in Fig. 9(a), the as-constructed electrolytic cell for NiFeZn/NiZn-Ni/NF-24h (+) || NiFeZn/NiZn-Ni/NF-24h (−) system only requires a low cell voltage of 1.588 V at 100 mA/cm^2. This performance surpasses that of the Pt/C/NF (+) || RuO_2/NF (−) system, which requires 1.805 V. The superior performance of NiFeZn/NiZn-Ni/NF-24h is further highlighted in Table S3 [36,42,47−49] in SI, where it outperforms the majority of comparable catalysts in the overall water splitting, underscoring its exceptional advantages as a bifunctional catalyst.

To explore the sustainable stability of NiFeZn/NiZn-Ni/NF-24h for hydrogen production, a chronopotentiometry test was conducted at a potential of

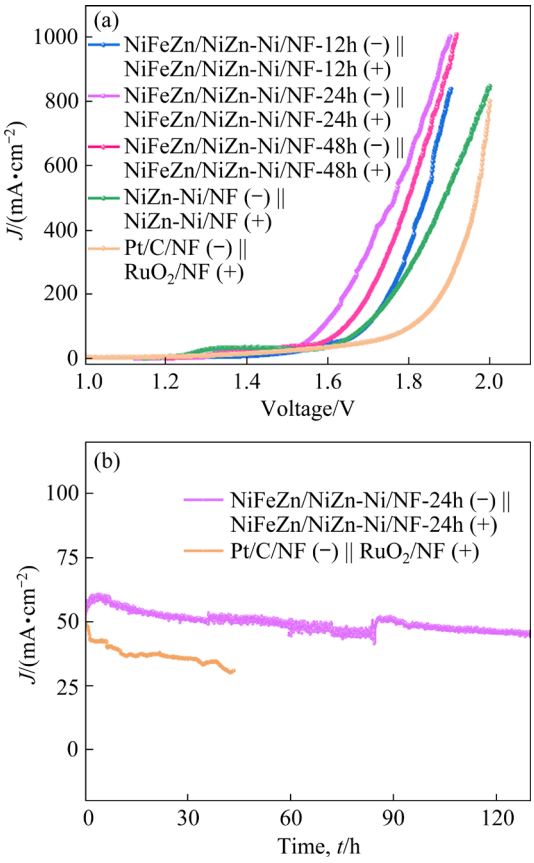

Fig. 9 LSV curves of as-prepared samples for overall water splitting (a) and chronoamperometric test results of NiFeZn/NiZn-Ni/NF-24h (+||−) and Pt/C/NF (+) || RuO_2/NF (−) at potential of 1.595 V in two-electrode system (b)

1.595 V over a continuous operation. As shown in Fig. 9(b), the catalyst maintained continuous water electrolysis for 120 h without significant current degradation, confirming its superior catalytic durability for overall water splitting. The low cell voltage and high stability of NiFeZn/NiZn-Ni/NF-24h make it an outstanding bifunctional electrocatalyst for overall water splitting, offering significant potential for practical applications in efficient and durable water electrolysis systems.

3.5 Morphology and structure of NiFeZn/NiZn-Ni/NF sample after long-term testing

SEM images of NiFeZn/NiZn-Ni/NF-24h sample after long-term HER and OER tests (Fig. 10) revealed that the original porous architecture well remained along with the formation of many nanosheet networks, which is often observed in NiFe-based catalysts due to the formation of oxides or hydroxides [50,51]. The XRD patterns of the NiFeZn/NiZn-Ni/NF-24h sample after the HER and OER tests also matched well with the initial ones (Fig. 11), manifesting its stable phase structure. Figures S8 and S9 in SI displayed the corresponding XPS data of Ni 2p, Fe 2p, Zn 2p, and O 1s after HER and OER tests, respectively. By careful comparison, the changes of Zn 2p and Ni 2p spectra can be ignored, while the content of Fe^{3+} species raised evidently, and the peak intensity of Fe^{2+} species decreased. For the O 1s spectrum, the proportion of M—OH bonds obviously increased and that of M—O bonds decreased significantly after HER and OER tests. The variations for Fe and

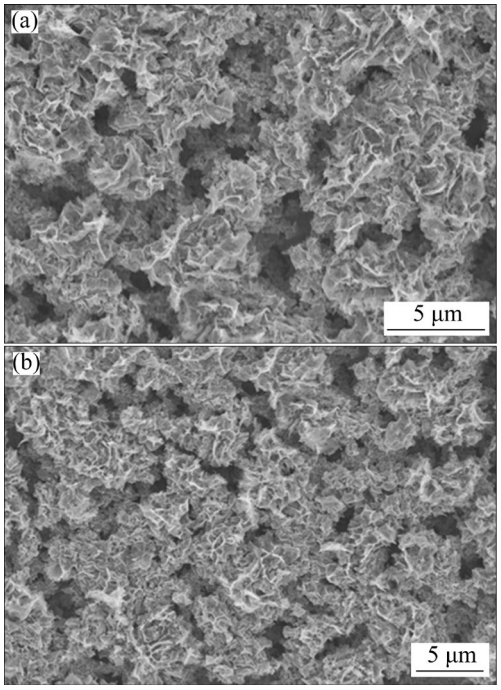

Fig. 10 SEM images of NiFeZn/NiZn-Ni/NF-24h sample after *J*–*t* test for HER (a) and OER (b)

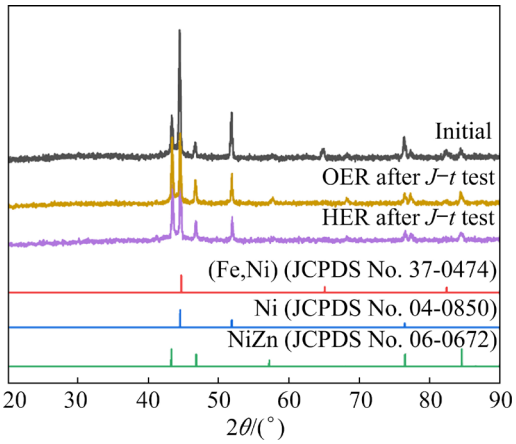

Fig. 11 XRD patterns of NiFeZn/NiZn-Ni/NF-24h sample before and after *J*–*t* test for HER and OER

O spectra suggested that many Fe atoms on the surface were further oxidized to form Fe—OOH during the long-term testing process [48,52]. The exceptional performance and stability of NiFeZn/NiZn-Ni/NF-24h can be attributed to its unique material structure and composition. These structural features likely enhance the catalytic activity and durability, making NiFeZn/NiZn-Ni/NF-24h a promising candidate for practical water splitting applications.

4 Conclusions

(1) A scalable and versatile dealloying strategy was developed to achieve in situ and seamless construction of double-layered multiscale porous NiFeZn/NiZn-Ni heterojunction via electroplating NiFeZn on NF followed by annealing and etching. This strategy could be extended to other materials and contexts.

(2) The modulation of the electronic structure through multi-interface engineering and the synergistic effects among Ni, Fe, and Zn significantly contribute to the advancement of catalytic materials, enhancing the intrinsic HER and OER activities.

(3) The integrated double-layered porous heterostructure with a 3D multiscale scaffold and hollow pore channels significantly enhances the efficiency and stability of catalytic processes by facilitating efficient transfer of electron and reactants/intermediates, maximally exposing catalytic sites, and improving structural stability during long-term HER and OER processes.

(4) The facile preparation and exceptional bifunctional performances of NiFeZn/NiZn-Ni hold prospect application potential for overall water splitting to hydrogen production.

CRediT authorship contribution statement

Ya-xin LI: Methodology, Data curation, Formal analysis, Writing − Original draft; **Hong-xiao YANG:** Investigation, Formal analysis; **Qiu-ping ZHANG:** Discussion, Formal analysis; **Tian-zhen JIAN:** Literature research, Formal analysis; **Wen-qing MA:** Formal analysis, Data curation; **Cai-xia XU:** Formal analysis, Data curation, Supervision, Writing − Review & editing; **Qiu-xia ZHOU:** Investigation, Data curation, Writing − Review & editing.

Declaration of competing interest

The authors declare that they have no known competing financial interests or personal relationships that could have appeared to influence the work reported in this paper.

Acknowledgments

This work was financially supported from the National Natural Science Foundation of China (No. 52201254), the Natural Science Foundation of Shandong Province, China (Nos. ZR2023ME155, ZR2020MB090, ZR2020QE012, ZR2020MB027), the Project of “20 Items of University” of Jinan, China (No. 202228046), and the Taishan Scholar Project of Shandong Province, China (No. tsqn202306226).

Supporting Information

Supporting Information in this paper can be found at: http://tnmsc.csu.edu.cn/download/18-p2972-2023-0207-Supporting_Information.pdf.

References

[1] CHEN Sheng, DUAN Jing-jing, JARONIEC M, QIAO Shi-zhang. Nitrogen and oxygen dual-doped carbon hydrogel film as a substrate-free electrode for highly efficient oxygen evolution reaction [J]. Advanced Materials, 2014, 26: 2925−2930.

[2] QI Jing, ZHANG Wei, CAO Rui. Solar-to-hydrogen energy conversion based on water splitting [J]. Advanced Energy Materials, 2018, 8: 1701620.

[3] TIAN Li-hong, YAN Xiao-dong, CHEN Xiao-bo. Electrochemical activity of iron phosphide nanoparticles in hydrogen evolution reaction [J]. ACS Catalysis, 2016, 6: 5441−5448.

[4] GODINEZ-SALOMON F, ALBITER L, ALIA S M, PIVOVAR B S, CAMACHO-FORERO L E, BALBUENA P B, MENDOZA-CRUZ R, ARELLANO-JIMENEZ M J, RHODES C P. Self-supported hydrous iridium-nickel oxide two-dimensional nanoframes for high activity oxygen evolution electrocatalysts [J]. ACS Catalysis, 2018, 8: 10498−10520.

[5] QIN Rong, HOU Jia-gang, XU Cai-xia, YANG Hong-xiao, ZHOU Qiu-xia, CHEN Zi-zhong, LIU Hong. Self-supporting $Co_{0.85}Se$ nanosheets anchored on Co plate as highly efficient electrocatalyst for hydrogen evolution reaction in both acidic and alkaline media [J]. Nano Research, 2020, 13: 2950−2957.

[6] SHEN Fang, JIANG Wen-jie, QIAN Guang-fu, CHEN Wei, ZHANG Hao, LUO Lin, YIN Shi-bin. Strongly coupled carbon encapsulated Ni−WO_2 hybrids as efficient catalysts for water-to-hydrogen conversion via urea electro-oxidation [J]. Journal of Power Sources, 2020, 458: 228014.

[7] SUN Jian-peng, QIN Shi-yu, MENG Xiang-chao. Joule heating-induced synthesis of Co−NC electrocatalyst for

hydrogen evolution reaction in seawater splitting [J]. Journal of Liaocheng University (Natural Science Edition), 2023, 36: 69−74. (in Chinese)

[8] LIU Xi-jun, XI Wei, LI Chao, LI Xi-bo, SHI Jing, SHEN Yong-li, HE Jia, ZHANG Li-han, XIE Lin, SUN Xiao-ming, WANG Peng, LUO Jun, LIU Li-min, DING Yi. Nanoporous Zn-doped Co_3O_4 sheets with single-unit-cell-wide lateral surfaces for efficient oxygen evolution and water splitting [J]. Nano Energy, 2018, 44: 371−377.

[9] LU Xue-feng, GU Lin-fei, WANG Jia-wei, WU Jun-xi, LIAO Pei-qin, LI Gao-ren. Bimetal-organic framework derived $CoFe_2O_4$/C porous hybrid nanorod arrays as high-performance electrocatalysts for oxygen evolution reaction [J]. Advanced Materials, 2017, 29: 1604437.

[10] LAI Tao, XU Ji-lin, XIAO Qi-fei, TONG Yun-xiang, HUANG Jun, ZHANG Jian-ping, LUO Jun-ming, LIU Yong. Preparation and characterization of porous NiTi alloys synthesized by microwave sintering using Mg space holder [J]. Transactions of Nonferrous Metals Society of China, 2021, 31: 485−498.

[11] DUAN Ran, LI Ye-jun, WANG Shu, TONG Yong-gang, RUBAHN H G, ZHANG Gu-fei, QI Wei-hong. Effects of phosphate precursors on morphology and oxygen evolution reaction activity of NiFe (oxy)hydroxide on nickel foams [J]. Transactions of Nonferrous Metals Society of China, 2022, 32: 4050−4061.

[12] WANG An-ling, XU Han, LI Gao-ren. NiCoFe layered triple hydroxides with porous structures as high-performance electrocatalysts for overall water splitting [J]. ACS Energy Letters, 2016, 1: 445−453.

[13] GAO Di, GUO Jiang-na, CUI Xun, YANG Lin, YANG Yang, HE Hui-chao, XIAO Peng, ZHANG Yun-huai. Three-dimensional dendritic structures of NiCoMo as efficient electrocatalysts for the hydrogen evolution reaction [J]. ACS Applied Materials & Interfaces, 2017, 9: 22420−22431.

[14] STASZAK-JIRKOVSKY J, MALLIAKAS C D, LOPES P P, DANILOVIC N, KOTA S S, CHANG K C, GENORIO B, STRMCNIK D, STAMENKOVIC V R, KANATZIDIS M G, MARKOVIC N M. Design of active and stable Co−Mo−S_x chalcogels as pH-universal catalysts for the hydrogen evolution reaction [J]. Nature Materials, 2016, 15: 197−203.

[15] ZHU Jia-wei, MU Shi-chun. Parsing the basic principles to build efficient heterostructures toward electrocatalysis [J]. Inorganic Chemistry Frontiers, 2023, 10: 2220−2225.

[16] JIAN Tian-zhen, MA Wen-qing, XU Cai-xia, LIU Hong, JOHN W. Intermetallic-driven highly reversible electro-catalysis in Li−CO_2 battery over nanoporous Ni_3Al/Ni heterostructure [J]. eScience, 2023, 3: 100114.

[17] LIU Yi-pu, LIANG Xiao, GU Lin, ZHANG Yu, LI Guo-dong, ZOU Xiao-xin, CHEN Jie-shen. Corrosion engineering towards efficient oxygen evolution electrodes with stable catalytic activity for over 6000 hours [J]. Nature Communications, 2018, 9: 2609.

[18] ZOU Xiao-xin, WU Yuan-yuan, LIU Yi-pu, LIU Da-peng, LI Wang, GU Lin, LIU Huan, WANG Peng-wei, SUN Lei, ZHANG Yu. In situ generation of bifunctional, efficient Fe-based catalysts from mackinawite iron sulfide for water splitting [J]. Chem, 2018, 4: 1139−1152.

[19] ZHU Jia-wei, GUO Yao, LIU Fang, XU Han-wei, GONG Lei, SHI Wen-jie, CHEN Ding, WANG Peng-yan, YANG Yue, ZHANG Cheng-tian, WU Jin-song, LUO Jia-huan, MU Shi-chun. Regulative electronic states around ruthenium/ruthenium disulphide heterointerfaces for efficient water splitting in acidic media [J]. Angewandte Chemie: International Edition, 2021, 60: 12328−12334.

[20] CHEN Ding, LIU Rui-hu, YU Ruo-han, DAI Yu-hang, ZHAO Hong-yu, WU Du-lan, WANG Peng-yan, ZHU Jia-wei, PU Zong-hua, CHEN Lei, YU Jun, MU Shi-chun. Work-function-induced interfacial built-in electric fields in Os−$OsSe_2$ heterostructures for active acidic and alkaline hydrogen evolution [J]. Angewandte Chemie: International Edition, 2022, 61: 202208642.

[21] ZHOU Meng, ZHU Zhi-jun, TANG Jian-guo, Electrodeposition preparation of iron cobalt nickel-based catalyst and application in oxygen evolution reaction [J]. Journal of Liaocheng University (Natural Science Edition), 2023, 36: 53−58. (in Chinese)

[22] ZHOU Qiu-xia, XU Cai-xia, HOU Jia-gang, MA Wen-qing, JIAN Tian-zhen, YAN Shi-shen, LIU Hong. Duplex interpenetrating-phase FeNiZn and $FeNi_3$ heterostructure with low-Gibbs free energy interface coupling for highly efficient overall water splitting [J]. Nano-micro Letters, 2023, 15: 95.

[23] ZHOU Qiu-xia, HAO Qin, LI Ya-xin, YU Jiang-hua, XU Cai-xia, LIU Hong, YAN Shi-shen. Free-standing trimodal porous NiZn intermetallic and Ni heterojunction as highly efficient hydrogen evolution electrocatalyst in the alkaline electrolyte [J]. Nano Energy, 2021, 89: 106402.

[24] WANG Hong-xia, CUI Mei-yan, FU Gao-liang, ZHANG Jia-ye, DING Xing-yu, IRENE A, MATTHEW B, DEMIE M K, VLADO K L, VICTOR A D O, FREDDY E O, KELVIN H L Z. Vertically aligned Ni/NiO nanocomposites with abundant oxygen deficient hetero-interfaces for enhanced overall water splitting [J]. Science China Chemistry, 2022, 65: 1885−1894.

[25] CHEN Ya-qiong, ZHANG Jin-feng, WAN Lei, HU Wen-bin, LIU Lei, ZHONG Cheng, DING Yi-da. Effect of nickel phosphide nanoparticles crystallization on hydrogen evolution reaction catalytic performance [J]. Transactions of Nonferrous Metals Society of China, 2017, 27: 369−376.

[26] LI Rui, XU Jing-song, LU Chao, HUANG Zhang-yong, WU Quan-wen, BA Jing-wen, TANG Tao, MENG Da-qiao, LUO Wen-hua. Amorphous NiFe phosphides supported on nanoarray-structured nitrogen-doped carbon paper for high-performance overall water splitting [J]. Electrochimica Acta, 2020, 357: 136873.

[27] ZHOU Qiu-xia, XU Cai-xia, LI Ya-xin, XIE Xi-miao, LIU Hong, YAN Shi-shen. Synergistic coupling of NiFeZn−OH nanosheet network arrays on a hierarchical porous NiZn/Ni heterostructure for highly efficient water splitting [J]. Science China Materials, 2022, 65: 1207−1216.

[28] LI Cong-ling, ZHANG Zhi-jie, LIU Rui. In situ growth of 3D NiFe LDH-POM micro-flowers on nickel foam for overall water splitting [J]. Small, 2020, 16: 2003777.

[29] LI Wen-long, LI Fu-sehng, ZHAO Yi-long, LIU Chang, LI Ying-zheng, YANG Hao, FAN Ke, ZHANG Pei-li, SHAN Yu, SUN Li-cheng. Promotion of the oxygen evolution performance of Ni−Fe layered hydroxides via the

introduction of a proton-transfer mediator anion [J]. Science China Chemistry, 2022, 65: 382−390.

[30] FENG Zhong-bao, LI Da-gang, WANG Lin, SUN Qiang, LU Pai, XING Peng-fei, AN Mao-zhong. In situ grown nanosheet NiZn alloy on Ni foam for high performance hydrazine electrooxidation [J]. Electrochimica Acta, 2019, 304: 275−281.

[31] LI Qun, WANG Xian-fu, TANG Kai, WANG Meng-fan, WANG Chao, YAN Cheng-lin. Electronic modulation of electrocatalytically active center of Cu_7S_4 nanodisks by cobalt-doping for highly efficient oxygen evolution reaction [J]. ACS Nano, 2017, 11: 12230−12239.

[32] LI Jing, CAI Wei-wei. Fabrication of hierarchical three-dimensional self-standing NiO_xH_y electrode toward efficient oxygen evolution reaction [J]. Journal of Liaocheng University (Natural Science Edition), 2023, 36: 11−16. (in Chinese)

[33] LIU Hao, XI Cong, XIN Jing-hua, ZHANG Guo-liang, ZHANG Shao-fei, ZHANG Zhi-jia, HUANG Qin, LI Jian-xin, LIU Hui, KANG Jian-li. Free-standing nanoporous NiMnFeMo alloy: An efficient non-precious metal electrocatalyst for water splitting [J]. Chemical Engineering Journal, 2021, 404: 126530.

[34] ZHANG Le, LIU Peng-fei, LI Yu-hang, WANG Wu-chong, ZU Meng-yang, FE Huai-qin, YANG Xiao-hua, YANG Hua-gui. Accelerating neutral hydrogen evolution with tungsten modulated amorphous metal hydroxides [J]. ACS Catalysis, 2018, 8: 5200−5205.

[35] ZHU Zheng-ju, YIN Hua-jie, HE Chun-ting, AL AMUN M, LIU Po-rui, JIANG Li-xue, ZHAO Yong, WANG Yun, YANG Hua-gui, TANG Zhi-yong, WANG Dan, CHEN Xiao-ming, ZHAO Hui-jun. Ultrathin transition metal dichalcogenide/3d metal hydroxide hybridized nanosheets to enhance hydrogen evolution activity [J]. Advanced Materials, 2018, 30: 1801171.

[36] LIU Hui-bing, GAO Jing, XU Xin-cheng, JIA Qiao-huan, YANG Liu, WANG Shi-tao, CAO Da-peng. Oriented construction Cu_3P and Ni_2P heterojunction to boost overall water splitting [J]. Chemical Engineering Journal, 2022, 448: 137706.

[37] WU Zheng-cui, ZOU Ze-xian, HUANG Jian-song, GAO Feng. $NiFe_2O_4$ nanoparticles/NiFe layered double-hydroxide nanosheet heterostructure array for efficient overall water splitting at large current densities [J]. ACS Applied Materials & Interfaces, 2018, 10: 26283−26292.

[38] YAO Meng-qi, HU Hao-hui, SUN Bao-long, WANG Ni, HU Wen-cheng, KOMARNENI S. Self-supportive mesoporous Ni/Co/Fe phosphosulfide nanorods derived from novel hydrothermal electrodeposition as a highly efficient electrocatalyst for overall water splitting [J]. Small, 2019, 15: 1905201.

[39] ZHANG Hao-jie, LI Xiao-peng, HAHNEL A, NAUMANN V, LIN Chao, AZIMI S, SCHWEIZER S L, MAIJENBURG A W, WEHRSPOHN R B. Bifunctional heterostructure assembly of NiFe LDH nanosheets on NiCoP nanowires for highly efficient and stable overall water splitting [J]. Advanced Functional Materials, 2018, 28: 1706847.

[40] TANG Jian, XU Ji-lin, LI Liang-liang, MA Yong-cun, YE Zhi-guo, LUO Hong-yu, LUO Jun-ming. In-situ hydrothermal synthesis of Ni−MoO_2 heterostructure on porous bulk NiMo alloy for efficient hydrogen evolution reaction [J]. Transactions of Nonferrous Metals Society of China, 2022, 32: 1598−1608.

[41] CHEN Jing, PAN An-qiang, ZHANG Wen-chao, CAO Xin-xin, LU Rong, LIANG Shu-quan, CAO Guo-zhong. Melamine-assisted synthesis of ultrafine Mo_2C/Mo_2N@N-doped carbon nanofibers for enhanced alkaline hydrogen evolution reaction activity [J]. Science China Materials, 2021, 64: 1150−1158.

[42] CAI Zheng-yang, BU Xiu-ming, WANG Ping, SU Wen-qiang, WEI Ren-jie, HO J C, YANG Jun-he, WANG Xian-ying. Simple and cost effective fabrication of 3D porous core-shell Ni nanochains@NiFe layered double hydroxide nanosheet bifunctional electrocatalysts for overall water splitting [J]. Journal of Materials Chemistry A, 2019, 7: 21722−21729.

[43] WANG Jie, LV Gui-cai, WANG Cheng. A highly efficient and robust hybrid structure of CoNiN@NiFe LDH for overall water splitting by accelerating hydrogen evolution kinetics on NiFe LDH [J]. Applied Surface Science, 2021, 570: 151182.

[44] ZHANG Rui, CHENG Lan-zi, WANG Zheng, KONG Fen-ying, TSEGAZAB Y, LV Wen-xin, WANG Wei. Ni_3S_2−Co_9S_8 heterostructure nanowires supported on Ni foam as highly efficient and stable electrocatalyst for oxygen evolution reaction [J]. Applied Surface Science, 2020, 526: 146753.

[45] HAO Ya-wen, DU Gao-hui, FAN Yi, JIA Li-na, HAN Di, ZHAO Wen-qi, SU Qiang-mei, XU Bing-she. Prussian blue analogues-derived Ni-doped $CoFe_2O_4$ hollow nanocubes as electrocatalysts for oxygen evolution reaction [J]. Applied Surface Science, 2023, 614: 156237.

[46] WU Xue-fei, LI Jun-wei, LI Yan, WEN Zhen-hai. NiFeP−MoO_2 hybrid nanorods on nickel foam as high-activity and high-stability electrode for overall water splitting [J]. Chemical Engineering Journal, 2021, 409: 128161.

[47] CAO Dong, XU Hao-xiang, CHENG Da-jian. Branch-leaf-shaped CuNi@NiFeCu nanodendrites as highly efficient electrocatalysts for overall water splitting [J]. Applied Catalysis B, 2021, 298: 120600.

[48] HU Jin, ZHU Sheng-li, LIANG Yan-qin, WU Shui-lin, LI Zhao-yang, LUO Shui-yuan, CUI Zhen-duo. Self-supported Ni_3Se_2@NiFe layered double hydroxide bifunctional electrocatalyst for overall water splitting [J]. Journal of Colloid and Interface Science, 2021, 587: 79−89.

[49] SUN Hua-chuan, LI Jian-gang, LV Lin, LI Zhi-shan, AO Xiang, XU Chen-hui, XUE Xin-ying, HONG Guo, WANG Chun-dong. Engineering hierarchical CoSe/NiFe layered-double-hydroxide nanoarrays as high efficient bifunctional electrocatalyst for overall water splitting [J]. Journal of Power Sources, 2019, 425: 138−146.

[50] CHEN Rong, HUANG Sung-fu, ZHOU Dao-jin, GAO Jia-jian, YANG Cang-jia, TAO Hua-bing, YANG Hong-bin, ZHANG Li-ping, ZHANG Lu-lu, XIONG Qi-hua, CHEN Hao-ming, LIU Bin. Layered structure causes bulk NiFe layered double hydroxide unstable in alkaline oxygen evolution reaction [J]. Advanced Materials, 2019, 31: 1903909.

[51] NIU Shuai, JIANG Wen-jie, TANG Tang, YUAN Lu-pan, LUO Hao, HU Jin-song. Autogenous growth of hierarchical NiFe(OH)$_x$/FeS nanosheet-on-microsheet arrays for synergistically enhanced high-output water oxidation [J]. Advanced Functional Materials, 2019, 29: 1902180.
[52] WU Jia-dong, WANG De-peng, WAN Shuao, LIU Hui-ling, WANG Cheng, WANG Xun. An efficient cobalt phosphide electrocatalyst derived from cobalt phosphonate complex for all-pH hydrogen evolution reaction and overall water splitting in alkaline solution [J]. Small, 2022, 18: 2202883.

原位构建多尺度、多孔 NiFeZn/NiZn-Ni 异质结用于高效全水解

李雅馨[1]，杨红晓[1]，张秋萍[1]，简天真[1]，马文庆[1]，徐彩霞[1]，周秋霞[2]

1. 济南大学 前沿交叉科学研究院(iAIR)，济南 250022；
2. 西南医科大学 医学信息与工程学院，泸州 646000

摘　要：开发高效非贵金属双功能电解水催化剂对于促进析氧反应(OER)和析氢反应(HER)的动力学至关重要。采用电沉积−退火−腐蚀策略，在泡沫镍(NF)表面原位制备一种具有三重异质界面的自支撑、多尺度多孔 NiFeZn/NiZn-Ni 异质结催化剂(NiFeZn/NiZn-Ni/NF)。独特的多界面工程和三维多孔骨架显著提高了物质传输效率，增强了电子相互作用，实现了超强的水分解双功能电催化性能。在碱性溶液中及 600 mA/cm²的电流密度下，NiFeZn/NiZn-Ni/NF 催化剂使 HER 和 OER 的过电位分别降低至 187 和 320 mV，且连续催化超过 150 h 几乎无活性损失。此外，使用 NiFeZn/NiZn-Ni/NF 作为阴极和阳极组装的电解槽分别在 1.796 和 1.901 V 的电池电压下获得了 600 和 1000 mA/cm^2 的电流密度，并在 50 mA/cm^2 电流密度和时间超过 100 h 条件下仍保持极高的稳定性。NiFeZn/NiZn-Ni/NF 作为低成本、高效的双功能催化剂在全水解领域显示出潜在的应用前景。

关键词：NiFeZn 合金；多重界面；多孔结构；脱合金化；全水解

(Edited by Wei-ping CHEN)